Applied Geochemistry 203 (2026) 106809

Contents lists available at ScienceDirect

Applied Geochemistry

journal homepage: www.elsevier.com/locate/apgeochem

Deciphering phosphorus dynamics in impacted river systems using phosphate oxygen and lead isotope analysis

Daren C. Gooddy [a,d,*], Andrew M. Tye [b], Andrew C. Smith [c], Simon R. Chenery [b], Benjamin JW. Surridge [d]

[a] UK Centre for Ecology & Hydrology, Maclean Building, Wallingford, Oxfordshire, OX10 8BB, UK
[b] British Geological Survey, Keyworth, Nottingham, NG12 5GG, UK
[c] NERC Environmental Isotope Facility, British Geological Survey, Keyworth, Nottingham, NG12 5GG, UK
[d] Lancaster Environment Centre, Lancaster University, Lancaster, LA1 4YQ, UK

ARTICLE INFO

Editorial handling by: Elisa Sacchi

Keywords:
Eutrophication
Phosphate oxygen isotopes
Lead isotopes
Sediment-water interaction

ABSTRACT

Phosphorus (P) is a major driver of eutrophication in river systems, but its sources and cycling remain poorly understood. This study employs a novel combination of phosphate oxygen isotope ($\delta^{18}O\text{-}PO_4$) and lead isotope ($^{206}Pb/^{207}Pb$) analyses to trace P sources and biogeochemical processes in river waters, shallow sediments (<5 cm), and sediment cores (up to 60 cm) along a ~100 km stretch of the River Nene, UK. $\delta^{18}O\text{-}PO_4$ signatures were used to identify phosphate origins and transformation pathways in river sediments, while $^{206}Pb/^{207}Pb$ ratios provided insights into sediment provenance and historical pollution. Results reveal significant spatial variability in P sources and sinks, with sewage inputs dominating in some parts, whereas and agricultural and urban contributions evident in others. Shallow (<5 cm) river sediment $\delta^{18}O\text{-}PO_4$ values are close to those in the overlying river water suggesting microbial cycling or some sorption to iron oxides at the river-sediment interface. Deeper sediments exhibit anthropogenic $^{206}Pb/^{207}Pb$ ratios throughout the core, with the $\delta^{18}O\text{-}PO_4$ shifts possibly influenced by organic matter decomposition and remineralisation. Sedimentary deposition conditions and permeability appear critical in determining the extent of mixing and diffusion between sediments and overlying water. These findings highlight the complex and dynamic interactions among microbial cycling, organic matter breakdown, iron reduction and reversible phosphate sorption processes. Integrating $\delta^{18}O\text{-}PO_4$ and $^{206}Pb/^{207}Pb$ analyses offers a potential framework for disentangling sediment-associated pollution and improving management of nutrient-enriched river systems.

1. Introduction

Phosphorus is a critical nutrient that supports the growth of aquatic organisms, particularly primary producers such as algae and aquatic plants. It plays a central role in ecosystem functioning by being a fundamental component of DNA, RNA, ATP, and cell membranes. However, the balance of phosphorus in aquatic systems is delicate, and overabundance can have severe environmental consequences. It is the rate-limiting factor for microbial and primary producer communities in many freshwater systems including rivers and streams (Sharpley et al., 2013).

Excessive phosphorus in river systems is a major driver of eutrophication, a process where nutrient enrichment leads to algal blooms, oxygen depletion, and the decline of aquatic biodiversity. Eutrophication affects water quality, fisheries, and the overall health of aquatic ecosystems. It is well established that high human population densities and intensive agriculture can lead to the oversupply of phosphorus to freshwaters, and result in eutrophication and a variety of other problems for the environment and human society (Schindler, 2012). Phosphorus inputs to rivers in agricultural catchments are usually dominated by diffuse sources related to various farming activities, but in more heavily populated catchments, point sources such as wastewater treatment works (WTWs) are of great importance (Howarth et al., 1996; Jordan et al., 1997; Jarvie et al., 2006; Palmer-Felgate et al., 2010). Understanding the relative contributions of these sources is vital for targeted mitigation efforts.

Once introduced into a river, phosphorus undergoes complex biogeochemical cycling, which are primarily influenced by 3 processes i)

* Corresponding author. UK Centre for Ecology & Hydrology, Maclean Building, Wallingford, Oxfordshire, OX10 8BB, UK.
E-mail address: dargoo@ceh.ac.uk (D.C. Gooddy).

https://doi.org/10.1016/j.apgeochem.2026.106809
Received 17 November 2025; Received in revised form 9 March 2026; Accepted 31 March 2026
Available online 1 April 2026

Sorption and desorption to sediment particles, particularly iron oxides ii) Microbial activity, including mineralisation and assimilation, and iii) Interactions with organic matter and redox processes. These interactions create spatial and temporal variability in phosphorus availability, making it challenging to predict its impacts and manage its inputs effectively. Hence, studying phosphorus dynamics is critical for developing evidence-based policies to reduce eutrophication and improve water quality.

Sediment phosphorus, stored in river systems is often referred to a legacy pollutant (Sharpley et al., 2013). It can influence the P status of river waters over long periods and will contribute to rivers failing 'Good Ecological Status' under the EU Water Framework Directive (EC. 2000). The 'equilibrium phosphate concentration (EPC_0)' concept (Froelich, 1988) explains why reductions in river water phosphate may result in the release of stored phosphate from the sediment.

Despite its importance, the sources, transformations, and sinks of phosphorus in river systems remain poorly understood. Traditional monitoring approaches often fail to distinguish between natural and anthropogenic contributions or to identify the mechanisms controlling its mobility and bioavailability. This limits the development of effective management strategies.

Phosphate oxygen isotopes ($\delta^{18}O\text{-}PO_4$) provide an opportunity to trace sources and study the biogeochemical cycling of P in waters (Davies et al., 2014; Gooddy et al., 2016, 2018) and sediments (Goldhammer et al., 2011; Yuan et al., 2019). Similarly, lead isotope ratios ($^{206}Pb/^{207}Pb$) can provide insights into the provenance of sediment-associated phosphorus, linking it to historical or ongoing pollution sources (Tye et al., 2021). Integrating these approaches offers a robust framework to disentangle the complex dynamics of phosphorus in river systems.

In an initial study, Tye et al. (2016) investigated P concentrations in sediments along a ~100 km section of the River Nene, a lowland river in the east of England. Results showed a trend in sediment P concentrations down the river system and 6 distinct water bodies. In the upper three water bodies (pre-urban areas) low concentrations of sediment-P were found reflecting the largely rural background and low soil erosion. However, the lower three water bodies had greatly enhanced sediment-P concentrations because of intensive arable agriculture with extensive under-field drainage acting as potential sediment sources, as well as 3 urban areas where major WTW's release treated water to the river.

A later study (Tye et al., 2021), using $^{206/207}Pb$ isotopes from petrol Pb as a tracer (along with relationships between P and other typical STW heavy metals released such as Sb, Zn, Cd) demonstrated that the cores sampled were largely of a historical nature, dating to a period before petrol Pb was phased out in 2000. Further, using $^{206/207}Pb$ isotopes for source apportionment, along with Monte-Carlo simulations and bootstrapping modelling methodologies, estimates of the sources of sediment-P were made. In the upper three water bodies, P was considered largely to be from soil, riverbank and channel sources with some input from a STW in waterbody 2, whilst approximately half of the phosphorus in sediment in the lower 3 water bodies were from diffuse (soil, banks etc) sources and half from STW sources.

In this study we use a set of depth profile cores taken during the initial study and combine $^{206/207}Pb$ isotope data with new $\delta^{18}O\text{-}PO_4$ data from both cores and river waters. The sediments have been extracted to release the non-labile P phases to better understand the degree and process by which legacy sediment P from historical anthropogenic inputs has been incorporated into the fixed sediment P pool over time, and whether it still has the potential to be involved in sediment-water interactions.

2. Materials and methods

2.1. Study area

The river Nene rises in Northamptonshire, flows in a north-easterly direction through the town of Northampton and City of Peterborough until it enters the Wash (Fig. 1). It is 161 km long with a total catchment area of 2270 km^2. It is a slow flowing river and historically has suffered from major siltation and macrophyte growth. The River Nene Catchment Board was formed in 1930 to enable extensive dredging and improved sediment management (Meadows, 2007). The non-tidal catchment is divided into six water bodies which have an area of 1590 km^2 (Fig. 1). The head waters have an altitude of ~160 m above ordnance datum (AOD), falling to ~6 m AOD at Peterborough. The largest fall occurs in the first 9.5 km, with the channel lying at 80 m AOD at the end of water body 1 (Meadows, 2007). The floodplain extends to 2 km at the widest point. The channel frequently bifurcates and is heavily engineered in sections (Williams and Fawthrop, 1988; Meadows, 2007). Major land use within the catchment is agriculture with arable (cereals and oilseed rape) and grassland dominating. Buffer strips are now commonly present on arable land adjacent to the river. Due to the heavy clay soils, the installation of drainage systems is common, with some discharging direct to the river as identified during the sediment sampling program. Several other smaller urban centres including are sited within the catchment (Fig. 1).

2.2. Sampling strategy

Full details of the sampling strategy can be found in previous studies on these cores (Tye et al., 2013; Tye et al., 2016). Six core samples were collected from each of the six Environment Agency designated WFD water bodies that make up the non-tidal section of the River Nene. The aim was to obtain robust estimates of sediment element concentrations with a reasonable estimate of variability (Tye et al., 2016). Whilst five of the collected sediment cores were homogenised prior to analysis, the sixth was divided into sections. This study focuses on this sixth core ($Core_D$) taken from each water body, which allowed elemental variations with depth to be examined (Tye et al., 2016). These cores are those numbered 2, 7, 15, 20, 28, 35 in Fig. 1.

For water bodies 1 & 2 and several samples of water body 3, the cores were collected by wading in the river. A boat was used to collect samples from water bodies 4, 5 and 6, and available launch sites in WB 4-6 partially determined the sites of core collection. A tour of sampling sites in the summer revealed that they were mainly covered in macrophytes (e.g. *Iris pseudacorus*).

Sampling took place following the very wet autumn/winter of 2012/13 in January and February 2013, a time of unusually long periods of flooding and high river flows. This was considered to have flushed significant sediment, with only well stabilised sediment deposits remaining, at least in the areas selected for sampling. Sediment flushing has previously been reported for the river Nene (Meadows, 2007). Cores were collected by pushing a length of polycarbonate tube (diameter = 58 mm internal diameter) into the sediment. Retention of the sediment was through a core catcher attached to the base of the tube. All cores were kept <4 °C after sampling and before drying. The total depth of sediment cores was recorded.

The core from each water body used in this analysis was cut into the five sections. The top section was always 0-5 cm as some of the sediment was used in measurements of EPC_0 to assess the rate at which P could be exchanged between the water and sediment and whether the sediment was acting as a source or sink (Tye et al., 2013). The remaining core was split into 4 equal sections and along with the remaining 0-5 cm section were air-dried (<30 °C) before being sieved to < 2 mm.

River water samples for $\delta^{18}O\text{–}PO_4$ and $\delta^{18}O\text{–}H_2O$ were collected subsequently (9th May 2023) to characterise the contemporary isotopic composition of river water and to provide a process-based reference against which sedimentary values could be interpreted. The purpose of this later sampling was not to obtain a time-matched snapshot of sediment inputs, but to constrain in-stream phosphate cycling, equilibrium relationships and potential exchange processes between water and sediments.

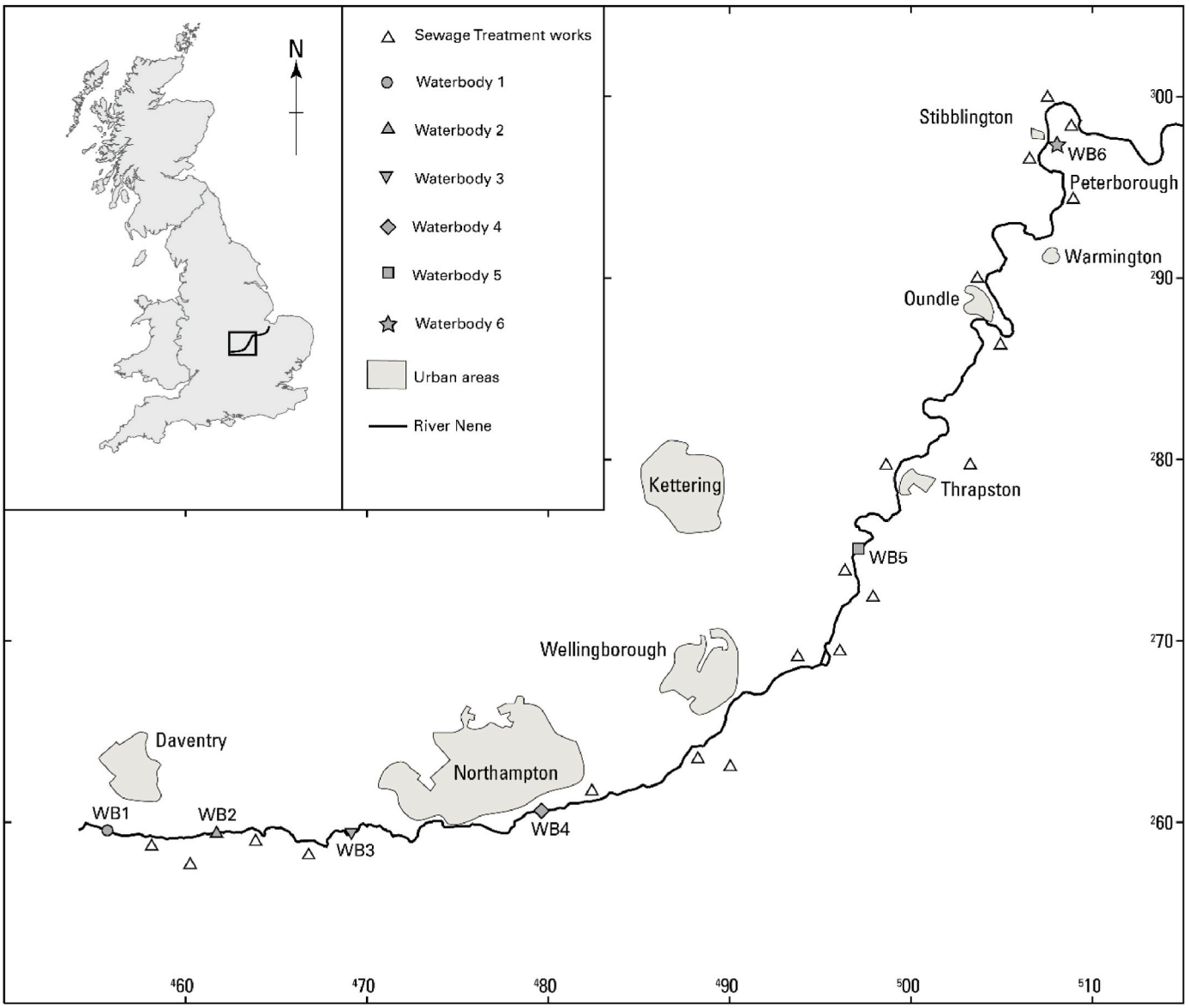

Fig. 1. Map of the study area and sampling locations in each of the water bodies of the River Nene. Sewage treatment works that discharge to the Nene are shown. Coordinates show kilometres of the British National Grid.

2.3. Analytical techniques

Total elemental (P, Fe, Mn, Pb) and Pb isotope analyses of the sediment were undertaken on dried and homogenised sediment subsamples (~30g), ground using an agate mill. Milled samples (<150 μm) were digested by weighing 0.25g of soil into a Savillex™ vial and adding HF, HNO_3 and $HClO_4$ concentrated and analytical grade acids. A stepped heating program up to 170 °C was used to digest silicate and oxide phases. The dry residue was re-constituted after warming with Milli-Q water, HNO_3 and H_2O_2, to 25 mL of 5 % v/v HNO_3 and stored in HDPE bottles. Reference materials (NIST SRM2710, SRM2711, GSS-6, BGS102 and BCR-2), duplicated samples and blanks were all prepared in a similar manner. Analysis was by ICP-MS in the British Geological Survey's (BGS) United Kingdom Accreditation Service (UKAS) and Monitoring Certification Scheme (MCERTS) accredited laboratory.

Sediment Pb isotope ratios were determined using an Agilent 7500 quadrupole ICP-MS. Preparation of the instrument for isotope ratio determinations involved the plateauing of the detector voltage, cross-calibration of the pulse counting-analogue modes and updating of the dead-time correction factors. Isotope ratio determinations consisted of 10 replicate integrations of 30s; each integration being 1000 peak jumps (1 point per peak) across the isotopes ^{206}Pb, ^{207}Pb and ^{208}Pb. Mass bias was addressed by using the isotope ratio for the reference material NIST SRM981, whilst correction factors were interpolated with reference to the accepted isotope ratios (Thirlwall, 2002). All samples were diluted to produce best counting statistics within the linear range of the pulse counting detector (<8000k cps). Quality control for Pb isotope ratios was performed using an in-house solution produced from a naturally occurring UK galena –"Glendenning" with long term (6 year) precision being 0.09% for $^{206}Pb/^{207}Pb$ and 0.11% for $^{208}Pb/^{207}Pb$ ratios. Individual sample errors in Pb isotope ratios were calculated by propagating the precision of individual sample measurements and the uncertainty in the measurements of the SRM981 sample. Typical sample uncertainties estimated were: 2SD $[^{206}Pb/^{207}Pb]$ = 0.009; 2SD $[^{208}Pb/^{207}Pb]$ = 0.015. Additional Pb isotope ratios (including $^{208}Pb/^{206}Pb$) and the full dataset for sediments and soils are provided in the Supplementary Information (Table S1; Fig. S1).

2.4. Stable isotope analysis

Freeze dried sediments were analysed for $\delta^{13}C$ and C/N % using an Elementar vario ISOTOPE cube coupled to an IsoPrime precisION gas chromatography combustion isotope ratio mass spectrometer at the British Geological Survey (Nottingham, UK), referencing certified material B2162 and BGS BROC3 as standards. Reproducibility for all isotope standards was within $\sigma \leq 0.1‰$ based on repeat analyses and C/N% accurate to 1%. Water oxygen isotope analysis ($\delta^{18}O$) was undertaken on an Isoprime Aquaprep coupled to an Isoprime 100 dual-inlet mass spectrometer through the headspace CO_2 equilibration with the water samples. Isotope ratios are reported as $\delta^{18}O–H_2O$ versus VSMOW, based on comparison with laboratory standards calibrated against IAEA standards VSMOW and SLAP, with analytical precision typically $\sigma \leq 0.05‰$.

Dried sediment samples were sequentially extracted to leave only the non-labile (operationally defined as HCl extractable) pool for purification to silver phosphate (Ag_3PO_4) and subsequent $\delta^{18}O\text{-}PO_4$ analysis. Simply, the bioavailable P pool was extracted and removed using anion resin strips, microbiological and metal bound P was removed using a combination of $NaHCO_3$ (0.5 M) and NaOH (0.1 M) and supernatants disposed of, before the non-labile pool was extracted using 100 ml of HCl (1 M). This extract was purified to silver phosphate following the method of Tamburini et al. (2010). One modification to this method was implemented, as in Pfahler et al. (2020), where 1 ml of concentrated H_2SO_4 was added during the ammonium phosphomolybdate (APM) step to ensure the pH remained at 1. The analysis of Ag_3PO_4 was undertaken by weighing approximately 200 μg of dried and ground sample Ag_3PO_4 into a capsule, in duplicate. The sample was converted to carbon monoxide (CO) using an Elementar PYRO cube elemental analyser at 1450 °C in the presence of carbon sources. The product CO was analysed on a Elementar isoprime vision IRMS. The $\delta^{18}O\text{-}PO_4$ values were calculated against two international Ag_3PO_4 standards B2207 (B2207 = $\delta^{18}O$ VSMOW value of +21.7‰) and USGS80 (USGS80 = $\delta^{18}O$ VSMOW value of +13.1‰) and internal Ag_3PO_4 standard, ALFA-2 (ALFA-2 = $\delta^{18}O$ VSMOW value of +14.2‰) was used as a check standard. Duplicate repeats had a typical precision $\sigma \leq 0.5‰$; furthermore, sample purity was assessed by determining the CO yield compared with the yield of Ag_3PO_4 standards (Expected O% of Ag_3PO_4 = 15.3%) and rejecting samples where this differed by 3%.

Two litre water samples were taken for the analysis of river water $\delta^{18}O\text{-}PO_4$, water sample phosphorus was concentrated using standard brucite precipitation methods. Simply, PO_4 was captured using a brucite brine (3 M $MgCl_2$ and 1 M NaOH solution), headspace water was removed and the brine centrifuged to concentrate, before being dissolved in 1 M HNO_3 (100 ml). This acidic solution was then used within the first step of the Tamburini et al. (2010) method (APM), and the same purification protocol used to convert this to Ag_3PO_4 as was used for the sediment samples. Isotope analysis was the same as detailed above.

2.5. Data analysis

Phosphate oxygen isotopes are a valuable tool in geochemical and biological studies because the oxygen atoms in phosphate can exchange with the surrounding water under certain conditions, particularly because of microbial activity. This exchange occurs when enzymes, such as phosphatases, catalyse the cleavage of phosphate bonds during the breakdown of organic phosphorus compounds or the recycling of inorganic phosphate. During these processes, the oxygen isotopes in the phosphate molecule interact with the oxygen isotopes in the surrounding water, eventually reaching isotopic equilibrium if the system is left undisturbed for sufficient time. The isotopic composition of phosphate oxygen thus reflects the environmental conditions, including temperature and microbial activity, at the time of equilibration (Paytan and McLaughlin, 2007; Blake et al., 2005). Equilibrium values are calculated based on the equation of Chang and Blake (2015):

$$\delta^{18}O_{PO4} = \left(\delta^{18}O_{H2O} + 1000\right) \times e^{\left[14.43\times\left(10^3/T\right)-26.54\right]/1000} - 1000 \quad (1)$$

where T is in degrees Kelvin.

3. Results

3.1. Water isotope data

The $\delta^{18}O\text{-}PO_4$ of water samples from each of the water bodies along the river Nene show considerable variation over the study area, ranging from a maximum of 18.8‰ in Waterbody 2, to a low of 10.2‰ in Waterbody 4 (Fig. 2). Similarly, $\delta^{18}O–H_2O$ values ranged from −7.1‰ in Water Body 1 to −6.3‰ in Water Bodies 4, 5 and 6. Temperature ranged from 12.2 °C in Water Body 1 to 15.8 °C in Water Bodies 5 and 6. Based on these values, the equilibrium value has a mean value of 17.2‰ ± 0.1‰ with Waterbodies 1 and 2 above the equilibrium and Waterbodies 3-6 below the equilibrium values. Waterbodies 3-6 fall below the range of values for calculated sediment equilibrium values (see full details of values in Fig. 2 caption) whereas Waterbodies 1 and 2 fall within this range. All measured values fall within the range experienced from a previous and extensive study of sewage treatment works outflows in the UK (Gooddy et al., 2018).

3.2. Sediments

Values for sediment carbon, nitrogen percentage and $\delta^{13}C$ taken as an average over the whole homogenised core are shown in Table 1. Unfortunately, there was insufficient sample to obtain values for some individual core depths. For the study area the mean carbon and nitrogen contents are 4.3% ± 1.7 and 0.3% ± 0.1 respectively. Waterbodies 1 and 2 have lower %C and %N than Waterbodies 3-6. The C/N ratio ranges from 11.6 to 24.5 (mean 14.9 ± 4.9) with the lowest value in Waterbody 1 and the highest in Waterbody 2. Similarly, the $\delta^{13}C$ ranges from −26.0‰ to −20.2‰ (mean −23.9‰±1.9), again with the lowest value in Waterbody 1 and the highest in Waterbody 2.

The relationship between water body $^{206/207}Pb$ isotope and $1/Pb_{total}$ for water body cores and selected adjacent soil sediments are shown in Fig. 3. Shaded areas show the isotopic range measured in UK leaded petrol and coal samples taken across England, primarily from coal beds in the English midlands ie within ~100-150 km of the river Nene. Samples from Water Bodies 1-3 and the nearby soils (from Water Bodies 1 and 3) all fall within the range found in coals from England, except for the top 0-5 cm of core from Water Body 3 and a topsoil from Water Body 1 which fall just outside of this range. The whole core from water body 4 is closer in range to values typically found in UK leaded petrol and much closer to values found for a sewage treatment works. The top 0-5 cm of core from Water Body 5 is similar in value to the whole core in Water Body 4. Deeper samples in Water Body 5 are close to, or within the range of English Coals, with the highest values associated with the deepest sediments. For water Body 6, deeper sediments between 20 and 65 cm fall within the range for coal, whereas the shallower sediments down to 20 cm fall a little below this range. Half of soils from within the reach of Water body 6 have coal-like values, with the lower Pb content corresponding to a lower P content, both of which are roughly 50% less than the non-coal like higher values. Additional Pb isotope ratios (including $^{208}Pb/^{206}Pb$) and the full dataset are provided in the Supplementary Information (Fig. S1; Table S1) and confirm the mixing relationships previously described for the Nene catchment (Tye et al., 2021).

Sediment profiles for total lead and isotopic content are shown in Fig. 4. Mean total lead contents are 22.6 mg/kg, 39.1 mg/kg, 56.9 mg/kg, 149 mg/kg, 102 mg/kg and 57.2 mg/kg for water bodies 1-6 respectively. Lead content of the sediments shows a moderate increase (around 20-50%) in concentration from the top to the bottom of the profiles for Water Bodies 1-4. Highest lead contents are in Water Body 4 which also show a gradually increasing trend in lead concentrations

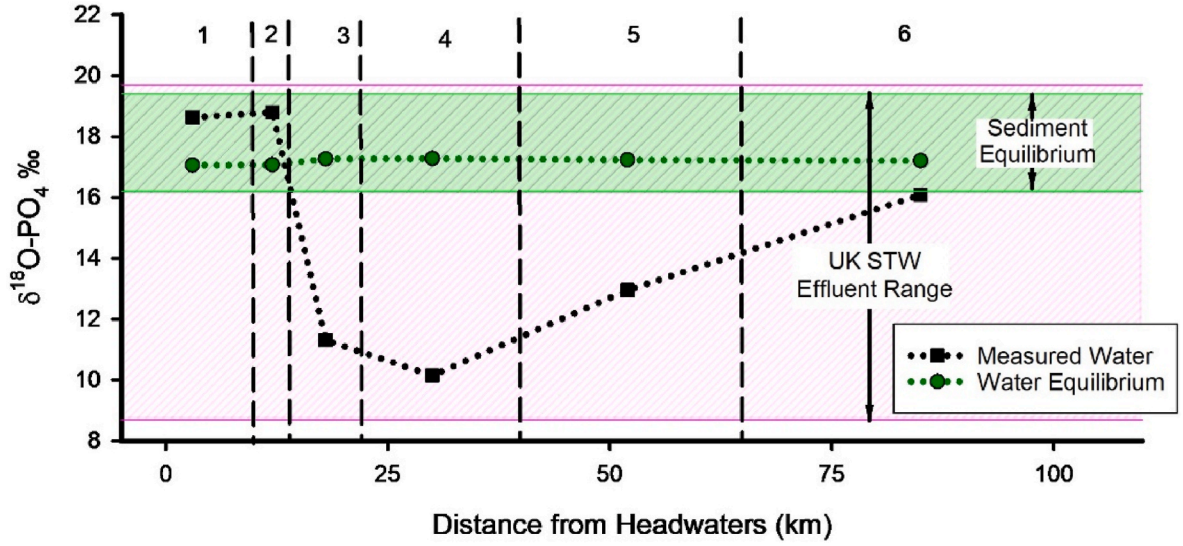

Fig. 2. Measured d18O-PO4 values for water in each water body compared with water equilibrium values, sediment equilibrium range (16.2 to 19.4‰) and UK sewage treat works range (8.7 to 19.7‰). Theoretical equilibrium is for sediments (green rectangle) given a range of temperatures (mean annual air temperature in Northampton of 4 to 17° and $\delta^{18}O$–H_2O from −6.3 to −7.1‰ as measured in this study) gives $\delta^{18}O$-PO_4 ranging for top sediments. Pink rectangle shows range of values observed from Sewage treatment works outflows from (Gooddy et al., 2018). (For interpretation of the references to colour in this figure legend, the reader is referred to the Web version of this article.)

Table 1
Concentration of C and Nitrogen and $\delta^{13}C$ composition of whole core samples taken in each water body.

Water body	Carbon	Nitrogen	C/N	$\delta^{13}C$
	%	%		‰
Average over core				
1	2.3	0.2	11.6	−26.0
2	2.0	0.1	24.5	−20.2
3	4.8	0.3	15.3	−24.1
4	5.8	0.4	13.3	−24.7
5	5.2	0.4	11.8	−23.9
6	5.8	0.4	13.1	−23.8

from top to bottom. In contrast, Water Body 5 show a rapid decrease down the profile, with lead contents decreasing by more than 60% from the top compared with the bottom.

The $^{206/207}Pb$ ratios for Water Body 1 and Water Body 2 show little deviation from around 1.18 (mean of 1.181 and 1.182 respectively). Water Body 3 shows a slight increase in the ratio from 1.169 to 1.188 (mean of 1.177). Data from all three of these cores falls into the older sediment bracket, close to those found in English coals. Water Body 4 shows a small but consistent fall in the ratio from 1.141 to 1.128 (mean of 1.131) which is much closer to a ratio typical of sewage or leaded petrol. By contrast, Water Body 5 (mean of 1.168) shows an increasing ratio with depth, starting at 1.134 and rapidly increasing to 1.170 within 5 cm, and ending at 1.185, suggesting significantly more English coal dominated and hence older sediments at depth. Water body 6 (mean of 1.170) also shows an increase in ratio with depth, although less marked than Water Body 5, starting at 1.160, below the range for coal, and increasing to 1.179 at the core base to be just inside the coal range.

Fig. 5 shows sediment core profiles for total phosphorus and phosphate oxygen isotopes. Mean total phosphorus contents are 1150 mg/kg, 3150 mg/kg, 2110 mg/kg, 4100 mg/kg, 2880 mg/kg and 1460 mg/kg for water bodies 1-6 respectively. Water Bodies 1 and 2 show an increasing trend in concentration with depth, more than doubling in Water Body 1 and rising by roughly 60% in Water Body 2. Water Body 3 concentrations show a slight decrease with depth, falling by roughly 20% from top to bottom of the profile. Water Body 4 increases by roughly 16% over the length of the profile, although the highest value is observed between 20 and 35 cm. A significant decrease is observed in concentrations from Water Body 5, falling by more than 50% over the entire core length, with most of that decrease (~40%) occurring between 0 and 20 cm. Concentrations of total Phosphorus decrease in a linear manner and fall by roughly 66% from the top to the bottom of the profile.

For $\delta^{18}O$-PO4, Water Bodies 1 and 2 show a decrease in values as a function of depth, with the fall in values particularly dramatic for Water Body 2. Water Body 3 shows a slight increase in values with depth, mirroring the slight decrease shown for P found here. Water Body 4 decreases with depth to a low value corresponding to the P high between 20 and 35 cm and then increases to a value higher than the top. Water Body 5 decreases in a similar way to P, with a large decrease in values from the top to the second sample between 5 and 20 cm. The core from Water Body 6 also behaves in a similar manner to that in Water Body 5, decreasing with depth but in a less linear manner than P and with a large drop in values from the top to the next sample below.

Profiles for total iron (Fe) and manganese (Mn) are shown in Fig. 6. Across all sites, Fe concentrations are roughly 10 times higher than Mn. Both elements generally increase with depth, more than doubling from the surface to the lowest part of the profile. Average Mn and Fe concentrations are 590 mg/kg and 50,900 mg/kg, respectively. In Water Body 2, Mn and Fe also increase with depth, with concentrations about twice as high as in Water Body 1. In Water Body 3, Mn decreases with depth, while Fe first increases, then decreases before slightly rising again. Mn concentrations (800 mg/kg) are similar to Water Body 1, while Fe concentrations (70,800 mg/kg) fall between those of Water Bodies 1 and 2. Water Body 4 shows Mn and Fe trends similar to Water Body 3, peaking between 20 and 35 cm, then decreasing before rising again at the base—mirroring the total phosphorus (P) pattern. Water Body 5 follows a similar pattern to Water Body 4, with Mn decreasing before a slight increase at 35–50 cm, then declining again. Fe remains relatively stable down to 20–35 cm before following the same increasing trend as Mn. In Water Body 6, Mn and Fe concentrations resemble those in Water Body 1. Mn decreases with depth, while Fe initially increases from shallow sediment before gradually declining.

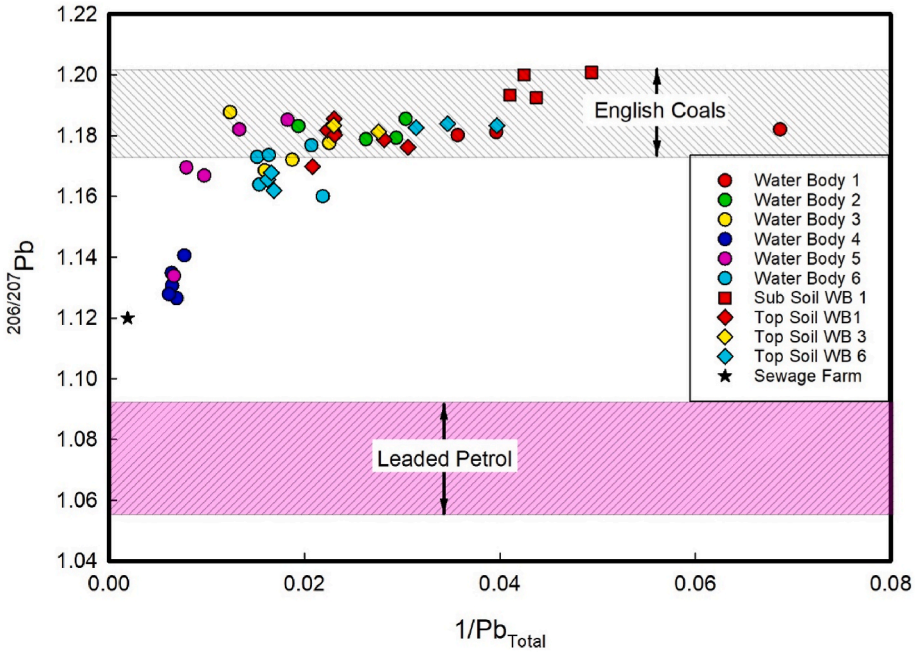

Fig. 3. $^{206/207}$Pb isotope ratios against the inverse of lead concentration for water bodies and soils in study sites along the River Nene. Ranges for leaded petrol are from Sugden et al. (1993) and for English coals from Farmer et al. (1999). Sewage farm sample taken from Atkinson et al. (2011). Top soil from WB1 (red diamond) is representative of the natural background. (For interpretation of the references to colour in this figure legend, the reader is referred to the Web version of this article.)

4. Discussion

The δ^{13}C values of river sediment provides insights into organic matter sources and carbon cycling, while C/N ratios help distinguish between terrestrial and microbial/algal contributions. Higher C/N ratios (~20) indicate terrestrial plant material, whereas lower values (~4-10) suggest algal or microbial sources (Meyers, 1994). For most of the Water Bodies, these values are similar, however Water Body 2 stands out, with much lower C and N contents and the lowest δ^{13}C. Hence, sediments in Water Body 2 have significantly different properties to the other Water Bodies which may reflect different inputs to the others.

It has previously been shown by Tye et al. (2021) that sources of P in the river sediment change as the river flows downstream. In Water Bodies 1-3, P comes from agricultural origin, and despite many STWs discharging into Water Bodies 3-6 (as shown by the δ^{18}O-PO$_4$ of the river water in Fig. 2), these only contribute ~50% of the sediment P within the system, the remainder coming from diffuse sources. The data show that for sediments in Water Bodies 4-6, the presence of Pb from leaded petrol more than 20 years after it was phased out, indicating stabilised river sediments being present for a long time, despite potential dredging and sediment management. With observable trends in Water Bodies 1-3, although the Pb isotopic values closer to those of nearby soils (Fig. 3) and hence a 'geogenic' $^{206/207}$Pb signature, these profiles are still representative of stabilised river sediments. The strong relationship between Pb, $^{206/207}$Pb and P suggest that the core samples represent historical inputs of Pb and P from a similar source (STW's) into the river, and there remains legacy P at depth.

The δ^{18}O-PO$_4$ value has been well established as a marker of STWs and many of the top sediment samples reflect these values. These 'source term' values are generally well preserved because there is an excess of P and microbial cycling may not significantly move that value towards equilibrium. However, except for the core from Water Body 3, δ^{18}O-PO$_4$ values decrease, often rapidly throughout the cores. This either suggests a significant shift in P sources over time, or a high degree of P processing or exchange.

The observed δ^{18}O-PO$_4$ values are exceptionally low. A study by Smith et al. (2021) suggests that values as low as this only come from igneous rocks, and this seems unlikely for a sedimentary system in the UK. It is also unlikely that this is a change in fertiliser usage since these come from P rich source rocks which generally have much higher δ^{18}O-PO$_4$ values ranging from 11.5 to 23.0 ‰ (Wells et al., 2022).

Many equilibrium-driven biogeochemical processes tend to shift δ^{18}O-PO$_4$ values towards equilibrium with ambient water, or produce enrichment relative to equilibrium. Enzymatic hydrolysis of inorganic phosphate leads to equilibrium with ambient water, enriching δ^{18}O-PO$_4$. For microbial equilibrium at 10 °C, δ^{18}O–H$_2$O would need to be between −20‰ and −22‰ to give equilibrium values around 2-4 ‰ (Chang and Blake, 2015). Precipitation of phosphate minerals typically preferentially incorporates lighter isotopes into the solid phase, leaving the dissolved pool enriched in ^{18}O. Similarly, dissolution of iron oxides releases adsorbed phosphate without significant isotope exchange, often revealing a residual pool with higher δ^{18}O-PO$_4$ (Jaisi et al., 2010). Organic phosphate remineralisation through microbial processes also raises δ^{18}O-PO$_4$ as phosphate equilibrates with intracellular water (Liang and Blake, 2006). Collectively, these processes generally drive δ^{18}O-PO$_4$ values upward in natural systems.

The observed low δ^{18}O-PO$_4$ values are unlikely to result from natural background sources and instead suggest influence from biogeochemical cycling. However, most known biogeochemical processes typically increase δ^{18}O-PO$_4$ values rather than decrease them especially to the very low values observed. Therefore, we propose an integrated mechanism driven by reducing conditions resulting from organic matter deposition and the reduction of Fe^{3+} to Fe^{2+} (see Fig. 7).

Organic matter and phosphate inputs from agricultural runoff, urban runoff, and sewage treatment works accumulate on the riverbed. With increasing depth, sediments become progressively oxygen-depleted due to the oxidation of organic matter at the surface. Concurrently, deeper sediments reflect progressively older periods of accumulation, as inferred from ^{206}Pb/^{207}Pb ratios in Water Bodies 5 and 6 that fingerprint historical petrol-derived Pb inputs (Fig. 4). This creates three distinct zones: an oxygenated surface layer, a transitional zone with diminishing oxygen (suboxic), and a fully anoxic zone.

The uppermost sediments are relatively well-oxygenated, and phosphate in these layers is either in equilibrium or approaching

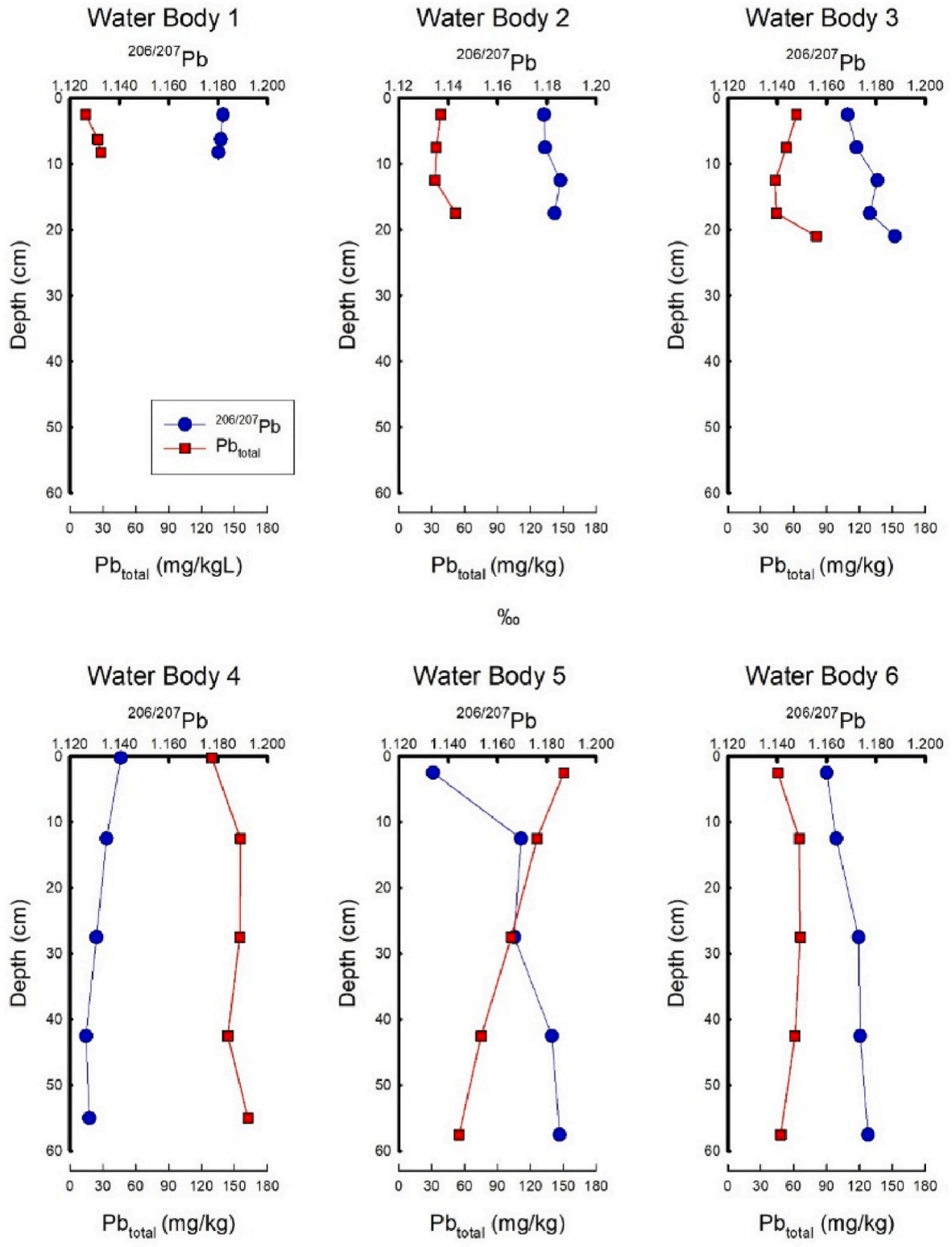

Fig. 4. Sediment profiles for total lead and $^{206/207}$Pb taken from 6 Water Bodies in the River Nene.

equilibrium with the overlying river water. In this zone, phosphate cycling is dominated by pyrophosphatase activity, with oxygen in the PO_4 molecule derived entirely from H_2O. δ^{18}O-PO_4 values in the top 5 cm of sediment range between 17.7‰ and 20.0‰.

An alternative, and not mutually exclusive, explanation for the observed low δ^{18}O-PO_4 values is enhanced phosphate regeneration and authigenic mineral formation under reducing sedimentary conditions. Previous experimental and field studies have demonstrated that phosphate released during organic matter remineralisation can deviate substantially from equilibrium δ^{18}O-PO_4 values (−7 to −20‰), reflecting kinetic isotope effects associated with enzymatic hydrolysis and incomplete intracellular oxygen exchange (Blake et al., 2005; Liang and Blake, 2006, 2009). In deeper sediments, supersaturation of porewater phosphate derived from organic P breakdown may promote the

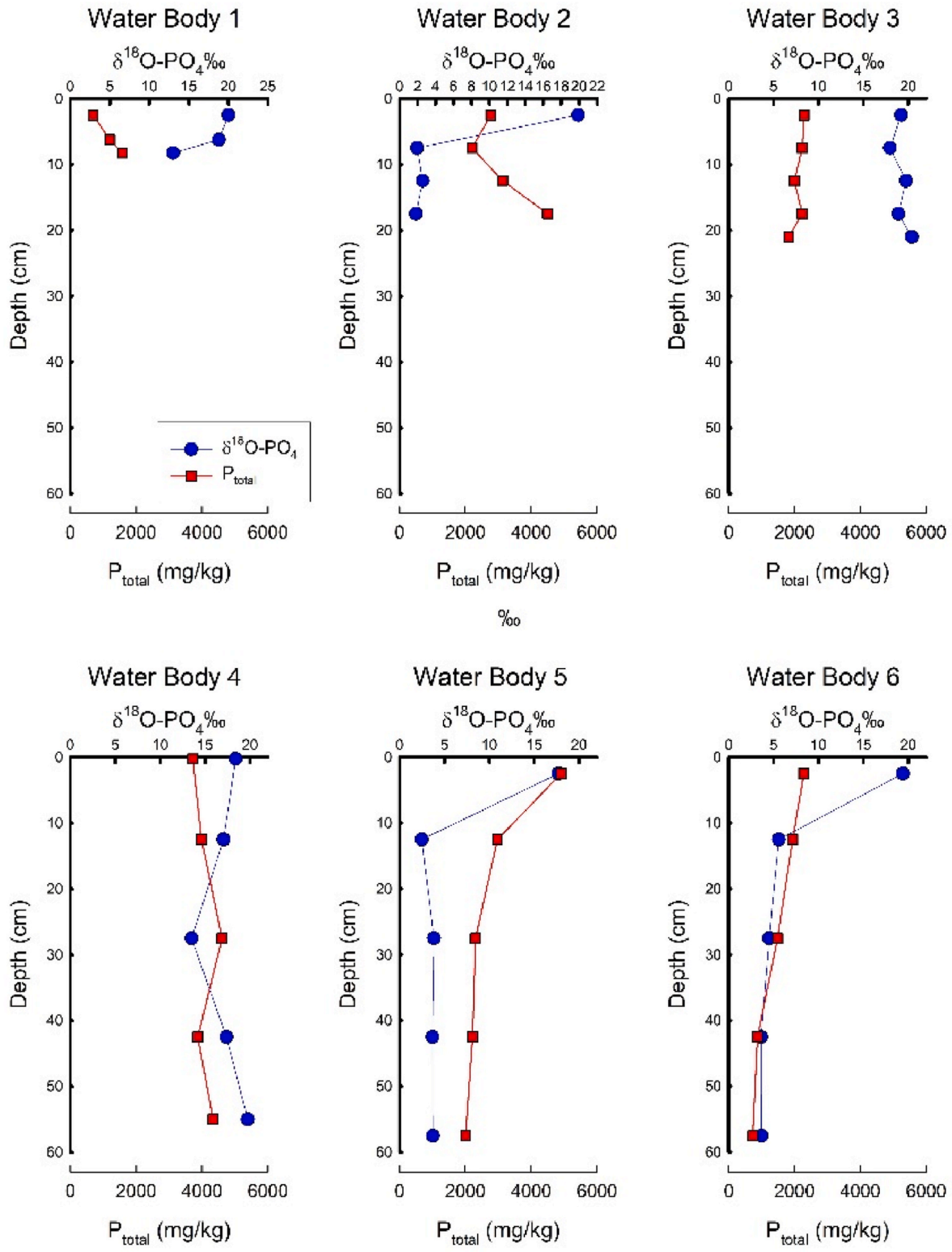

Fig. 5. Sediment profiles for total phosphorus and $\delta^{18}O\text{-}PO_4$ taken from 6 Water Bodies in the River Nene.

precipitation of authigenic phosphate phases through a series of intermediate species or precursors. Phosphate incorporated into these mineral phases may retain low, non-equilibrium $\delta^{18}O\text{-}PO_4$ signatures, particularly where microbial turnover is limited and exchange with overlying river water is restricted. As the $\delta^{18}O\text{-}PO_4$ values reported here derive from the HCl-extractable fraction, which likely integrates authigenic and detrital phosphate pools, these processes provide a plausible mechanism for the preservation of isotopically light phosphate at depth.

In addition to these regeneration and authigenic precipitation pathways, iron redox cycling exerts an important secondary control on phosphate mobility and isotopic preservation within the sediment profile. Beneath the surface layer, the reduction of sedimentary Fe_2O_3 (containing insoluble Fe^{3+}) to Fe^{2+} under increasingly anoxic conditions promotes the release of mineral-bound phosphorus and alters porewater

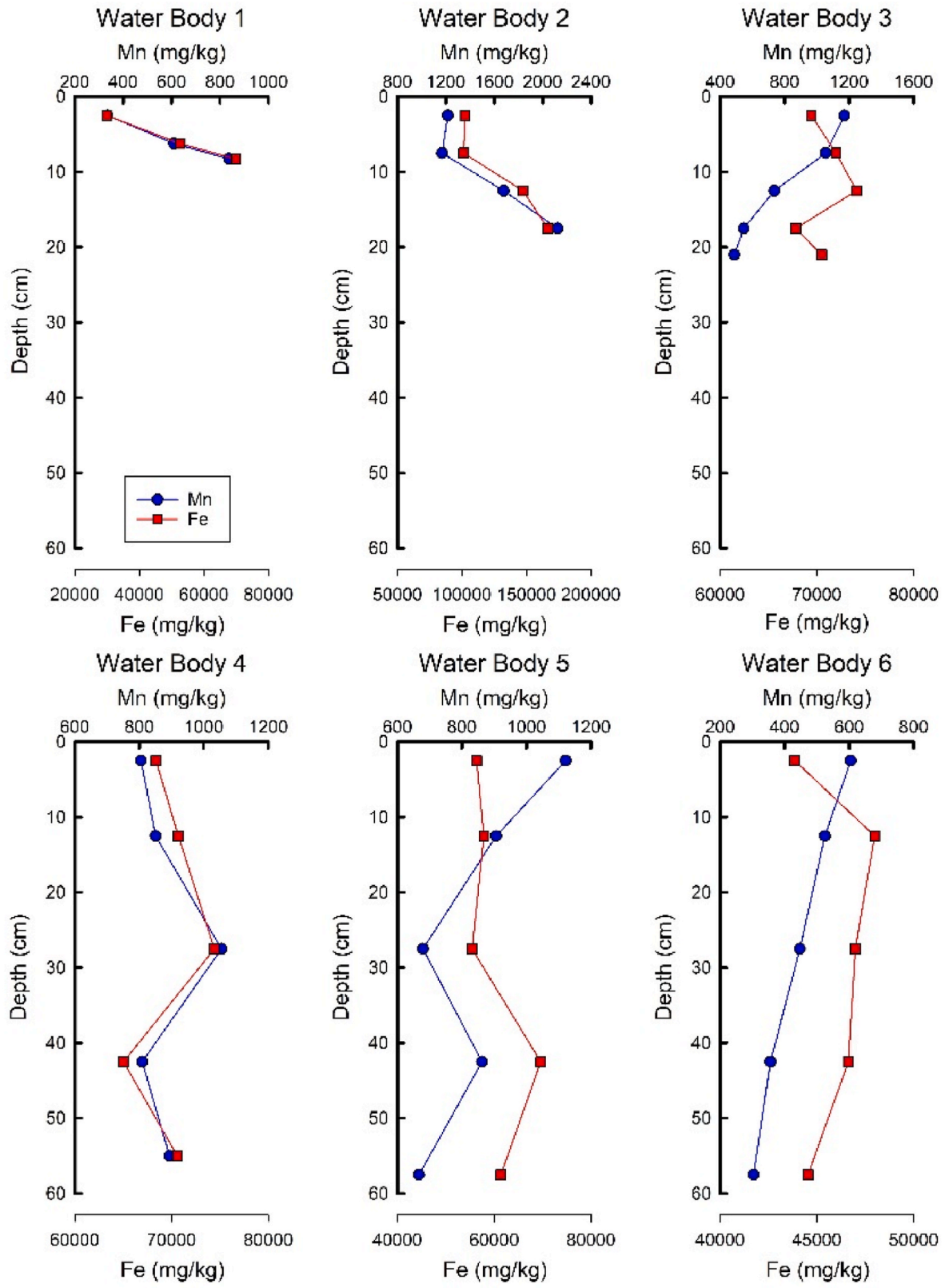

Fig. 6. Sediment profiles for total iron and total manganese taken from 6 Water Bodies in the River Nene.

chemistry. Phosphate released under these conditions may form PO_4 either enzymatically, tending to increase $\delta^{18}O\text{-}PO_4$ towards equilibrium, or through abiotic pathways that preserve non-equilibrium isotope signatures. As depth increases, porewaters become progressively more isolated from overlying river water due to lower permeability and reduced diffusion, limiting subsequent isotopic re-equilibration. Under these conditions, iron reduction facilitates phosphate release while promoting the retention of isotopically light $\delta^{18}O\text{-}PO_4$ values generated earlier during regeneration or mineral precipitation processes. The observed decline in total iron concentrations with depth in Water Bodies

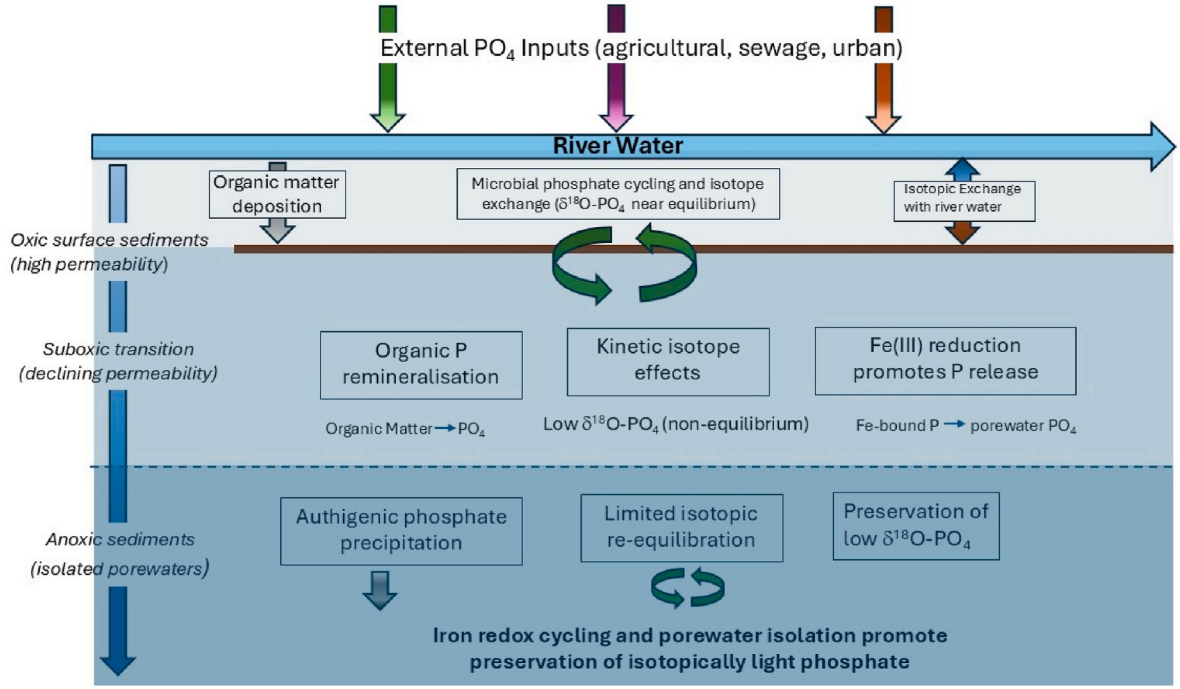

Fig. 7. Conceptual model illustrating the combined controls on sedimentary phosphate cycling and $\delta^{18}O\text{-}PO_4$ signatures under progressively reducing conditions within the sediment profile. Organic matter deposition drives oxygen depletion with depth, leading to a transition from oxic to suboxic and anoxic conditions. In surface sediments, phosphate undergoes active microbial cycling and isotopic exchange with overlying river water, resulting in $\delta^{18}O\text{-}PO_4$ values close to equilibrium. At greater depths, organic P remineralisation and authigenic phosphate formation under non-equilibrium conditions can generate isotopically light $\delta^{18}O\text{-}PO_4$ values. Concurrent iron(III) reduction facilitates the release of mineral-bound phosphate and, together with decreasing permeability and porewater isolation, limits subsequent isotopic re-equilibration. Iron redox cycling is therefore interpreted as a secondary control that promotes the preservation of low $\delta^{18}O\text{-}PO_4$ signatures generated during regeneration and mineral precipitation processes, rather than a direct oxygen source for phosphate formation.

5 and 6 is consistent with Fe^{3+} consumption and Fe^{2+} release, supporting the role of iron reduction as a key control on phosphate cycling and preservation within deeper sediments (Fig. 6).

While this mechanism is plausible for Water Bodies 5 and 6, it does not fully account for observations in other systems.

Water Body 1 shows a decrease in $\delta^{18}O\text{-}PO_4$ to ~13‰ alongside increasing Fe concentrations and little change in $^{206}Pb/^{207}Pb$. However, this $\delta^{18}O\text{-}PO_4$ value remains within the credible range for STW effluent. Additionally, the sediment core here is relatively short, which may limit interpretation.

Water Body 2 exhibits a sharp drop in $\delta^{18}O\text{-}PO_4$ to values well below those typical for STW effluent. Although Fe concentrations increase with depth, they are approximately twice as high as in other water bodies. This suggests the signal from iron reduction may be obscured by other processes or excess iron inputs.

Water Body 3 displays progressively older sediments with depth, yet $\delta^{18}O\text{-}PO_4$ values remain stable. While Fe concentrations stay constant, Mn levels decline sharply, implying mildly reducing conditions sufficient for Mn oxide reduction but insufficient to mobilize Fe.

Lastly Water Body 4, based on $^{206}Pb/^{207}Pb$ data, appears to have experienced more recent sediment deposition. There is little variation in $\delta^{18}O\text{-}PO_4$ values with depth, which may suggest that reaction kinetics are slow, preventing significant isotopic modification over the observed timescales.

While typical biogeochemical processes tend to elevate $\delta^{18}O\text{-}PO_4$ values, the observed depletion suggests an alternative mechanism. Clearly varying patterns across other water bodies indicate additional or overlapping processes, highlighting the complexity of phosphorus cycling in sedimentary environments influenced by anthropogenic and natural inputs. The sedimentary deposition conditions, which differ significantly between the sites, leading to permeability variations and reduction, appear critical in determining the extent of mixing and diffusion between sediments and overlying water and interstitial porewater.

5. Conclusions

Through a comprehensive geochemical and isotopic analysis of sediments from the River Nene, this study highlights the persistence and complexity of legacy phosphorus (P) in lowland river systems under varying land-use pressures. The combined use of phosphate oxygen isotopes ($\delta^{18}O\text{–}PO_4$) and lead isotopes ($^{206}Pb/^{207}Pb$) provides complementary information, with Pb isotopes constraining the timing and sources of sediment accumulation and $\delta^{18}O\text{–}PO_4$ reflecting phosphate cycling and regeneration processes occurring within that sedimentary framework. In this context, upstream rural sediments are predominantly influenced by diffuse inputs, whereas downstream urbanised reaches show a substantial contribution from sewage-derived material, supported by elevated Pb concentrations and isotope signatures consistent with historical petrol inputs. The persistence of petrol-derived Pb decades after its phase-out indicates that sediment-bound P is stable and long-lived, forming a legacy P pool that may continue to influence water quality.

Furthermore, $\delta^{18}O\text{-}PO_4$ profiles revealed that while surface sediments reflect STW-derived phosphate, deeper layers exhibit anomalously low $\delta^{18}O\text{-}PO_4$ values not easily attributed to known natural or anthropogenic sources. These low values likely reflect phosphate regeneration and mineral precipitation under reducing conditions, where kinetic isotope effects and restricted exchange limit equilibration with ambient water. Further work is required to better understand the full nature of these interactions. The study underscores the importance of biogeochemical transformations in modulating P availability and isotopic signatures in river sediments over time. Collectively, these results suggest that effective river management strategies must address

both current inputs, and the legacy contaminants in sediments, requiring more nuanced approaches to reduce eutrophication risk and achieve long-term improvements in ecological status.

CRediT authorship contribution statement

Daren C. Gooddy: Conceptualization, Funding acquisition, Investigation, Methodology, Project administration, Writing – original draft, Writing – review & editing. **Andrew M. Tye:** Data curation, Formal analysis, Investigation, Writing – review & editing. **Andrew C. Smith:** Data curation, Formal analysis, Investigation, Methodology, Writing – original draft, Writing – review & editing. **Simon R. Chenery:** Data curation, Formal analysis, Writing – review & editing. **Benjamin JW. Surridge:** Formal analysis, Writing – review & editing.

Declaration of competing interest

The authors declare that they have no known competing financial interests or personal relationships that could have appeared to influence the work reported in this paper.

Acknowledgements

The authors would like to thank the UK Environment Agency for funding the initial work and core collection (Project Reference 30258). NERC Environmental Isotope Facility (NEIF) grant 2465.1021 supported the phosphate isotope work. AT has received time from NERC Grant AgZero + for manuscript preparation. AT and AS publish with the permission of the Executive Director, BGS.

Appendix A. Supplementary data

Supplementary data to this article can be found online at https://doi.org/10.1016/j.apgeochem.2026.106809.

Data availability

Data will be made available on request.

References

Atkinson, N.R., Bailey, E.H., Tye, A.M., Breward, N., Young, S.D., 2011. Fractionation of lead in soil by isotopic dilution and sequential extraction. Environ. Chem. 8, 493–500.

Blake, R.E., O'Neil, J.R., Surkov, A.V., 2005. Biogeochemical cycling of phosphorus: insights from oxygen isotope effects of phosphoenzymes. Am. J. Sci. 305 (6-8), 596–620.

Chang, S.J., Blake, R.E., 2015. Precise calibration of equilibrium oxygen isotope fractionations between dissolved phosphate and water from 3 to 37 °C. Geochem. Cosmochim. Acta 150, 314–329.

Davies, C.L., Surridge, B.W.J., Gooddy, D.C., 2014. Phosphate oxygen isotopes within aquatic ecosystems: global data synthesis and future research priorities. Sci. Total Environ. 496, 563–575.

EC, 2000. Directive 2000/60/EC of the European parliament and of the council establishing a framework for the community action in the field of water policy. Official Journal L 327, 0001-0073 (22/12/2000), Brussels, Belgium.

Farmer, J.G., Eades, L.J., Graham, M.C., 1999. The lead content and isotopic composition of British coals and their implications for past and present releases of lead to the UK environment. Environ. Geochem. Health 21, 257–272.

Froelich, P.N., 1988. Kinetic control of dissolved phosphate in natural rivers and estuaries: a primer on the phosphate buffer mechanism. Limnol. Oceanogr. 33, 649–668.

Goldhammer, T., Brunner, B., Bernasconi, S.M., Ferdelman, T.G., Zabel, M., 2011. Phosphate oxygen isotopes: insights into sedimentary phosphorus cycling from the Benguela upwelling system. Geochem. Cosmochim. Acta 75, 3741–3756.

Gooddy, D.C., Bowes, M.J., Lapworth, D.J., Lamb, A.L., Williams, P.J., Newton, R.J., Davies, C.L., Surridge, B.W.J., 2018. Evaluating the stable isotopic composition of phosphate oxygen as a tracer of phosphorus from waste water treatment works. Appl. Geochem. 95, 139–146.

Gooddy, D.C., Lapworth, D.J., Bennett, S.A., Heaton, T.H.E., Williams, P.J., Surridge, B. W.J., 2016. A multi-stable isotope framework to understand eutrophication in aquatic ecosystems. Water Res. 88, 623–633.

Howarth, R.W., Billen, G., Swaney, D., Townsend, A., Jaworski, N., Lajtha, K., et al., 1996. Regional nitrogen budgets and riverine N & P fluxes for the drainages to the North Atlantic Ocean: natural and human influences. Biogeochem. 35, 75–139.

Jaisi, D.P., Blake, R.E., Kukkadapu, R.K., 2010. Fractionation of oxygen isotopes in phosphate during its interaction with iron oxides. Geochem. Cosmochim. Acta 74, 1309–1319.

Jarvie, H.P., Neal, C., Withers, P.J.A., 2006. Sewage-effluent phosphorus: a greater risk to river eutrophication than agricultural phosphorus. Sci. Total Environ. 360, 246–253.

Jordan, E.T., Correll, D.L., Weller, D.E., 1997. Relating nutrient discharges from watersheds to land use and streamflow variability. Water Resour. Res. 33, 25779-2590.

Liang, Y., Blake, R.E., 2006. Oxygen isotope of Pi regeneration from organic compounds by phophomonesterases and photooxidation. Geochem. Cosmochim. Acta 70, 3957–3969.

Liang, Y., Blake, R.E., 2009. Compound- and enzyme-specific phosphodiester hydrolysis mechanisms revealed by d18O of dissolved inorganic phosphate: implications for marine P cycling. Geochem. Cosmochim. Acta 73, 3782–3794.

Meadows, I., 2007. Hydrology. In: Allen, P., Boismier, W.A., Brown, A.G., Chapman, A., Meadows, I. (Eds.), Synthetic Survey of the Environmental Archaeological and Hydrological Record for the River Nene from its Source to Peterborough. Northamptonshire Archaeology. Report PNUM 3453, UK.

Meyers, P.A., 1994. Preservation of elemental and isotopic source identification of sedimentary organic matter. Chem. Geol. 114 (3-4), 289–302.

Palmer-Felgate, E.J., Mortimer, R.J.G., Krom, M.D., Jarvie, H.P., 2010. Impact of point-source pollution on phosphorus and nitrogen cycling in stream-bed sediments. Environ. Sci. Technol. 443, 908–914.

Paytan, A., McLaughlin, K., 2007. The oceanic phosphorus cycle. Chem. Rev. 107, 563–576.

Pfahler, V., Macdonald, A., Mead, A., Smith, A.C., Tamburini, F., Blackwell, M.S.A., Granger, S.J., 2020. Changes of oxygen isotope values of soil P pools associated with changes in soil pH. Sci Reports 10 (1), 2065.

Schindler, D.W., 2012. The dilemma of controlling cultural eutrophication of lakes. Proc. R. Soc. A B 279 (1746), 4322–4333.

Sharpley, A., Jarvie, H.P., Buda, A., May, L., Spears, B., Kleinman, P., 2013. Phosphorus legacy: overcoming the effects of past management practices to mitigate future water quality impairment. J. Environ. Qual. 42, 1308–1326.

Smith, A.S., Pfahler, V., Tamburini, F., Blackwell, M.S.A., Granger, S.J., 2021. A review of phosphate oxygen isotope values in global bedrocks: characterising a critical endmember to the soil phosphorus system. J. Plant Nutr. Soil Sci. 184, 25–34.

Sugden, C.L., Farmer, J.G., MacKenzie, A.B., 1993. Isotopic ratios of lead in contemporary environmental material from Scotland. Environ. Geochem. Health 15, 59–65.

Tamburini, F., Bernasconi, S.M., Angert, A., Weiner, T., Frossard, E., 2010. A method for the analysis of the δ18O of inorganic phosphate extracted from soils with HCl. Eur. J. Soil Sci. 61, 1025–1032.

Thirlwall, M.F., 2002. Multicollector ICP-MS analysis of Pb isotopes using a ^{207}Pb-^{204}Pb double spike demonstrates up to 400 ppm/amu systematic errors in Tl-normalization. Chem. Geol. 184, 255–279.

Tye, A.M., Chenery, S., Cave, M.R., Price, R., 2021. Using $^{206/207}Pb$ isotope ratios to estimate phosphorus sources in historical sediments of a lowland river system. J. Soils Sediments 21, 613–626.

Tye, A.M., Hurst, M.D., Barkwith, A.K.A.P., 2013. Nene Phosphate in Sediment Investigation – Environment Project REF:30258, Open Access Report OR/13/031. BGS, UK.

Tye, A.M., Rawlins, B.G., Rushton, J.C., Price, R., 2016. Understanding the controls on sediment-P interactions and dynamics along a non-tidal river system in a rural-urban catchment: the River Nene. Appl. Geochem. 66, 219–233.

Wells, N.S., Gooddy, D.C., Reshid, M.Y., Williams, P.J., Smith, A.C., Eyre, B.D., 2022. $\delta^{18}O$ as a tracer of PO_4 losses from agricultural landscapes. J. Environ. Manag. 317, 115299.

Williams, J.J.R., Fawthrop, N.P., 1988. A mathematical hydraulic model of the River Nene – a canalized and heavily controlled river. Regul. Rivers 2, 517–533.

Yuan, H., Li, Q., Kukkadapu, R.K., Liu, E., Yu, J., Fanf, H., Li, H., Jaisi, D.P., 2019. Identifying sources and cycling of phosphorus in the sediment of a shallow freshwater lake in China using phosphate oxygen isotopes. Sci. Total Environ. 676, 823–833.